Journal of
Marine Science and Engineering

MDPI

Article

Proposed Z-Source Electrical Propulsion System of a Fuel Cell/Supercapacitor-Powered Ship

Shihong Gan *, Weifeng Shi and Xiaoyan Xu

Electrical Engineering Department, Shanghai Maritime University, Shanghai 201306, China; wfshi@shmtu.edu.cn (W.S.); xuxy@shmtu.edu.cn (X.X.)
* Correspondence: shgan@shmtu.edu.cn

Abstract: The use of green energy to power ships in the marine industry has attracted increasing attention in recent years. This paper presents an inland river cruise ship supplied by a fuel cell (FC) as the main power source and a supercapacitor (SC) as the auxiliary power source. Its propulsion inverter adopts the proposed high-boost Z-source inverter, and the proposed high-voltage-boost Z-source inverter (HVB-ZSI) principle is studied. The advantages of this proposed HVB-ZSI in two cases are verified through simulation. In case 1, it can be seen that the capacitance voltage is only 250 V, and the maximum inductance's inrush current at the start is less than 200 A. But the capacitance voltage of HVB-ZSI reaches 383 V, and the inrush current is 300 A. While considering different constraints of the propulsion system, four operating modes for the set of the FC and SC are proposed. The small-signal model of the propulsion system is derived, and the control strategy is studied. By controlling the shoot-through duty cycle and modulation factor, the FC power, output power, and state of charge (SOC) of the SC can be controlled. Finally, to verify the performance of the proposed propulsion system, a hybrid power ship prototype equipped with a 7.5 kw propulsion motor is constructed. Four modes of the entire system are simulated by MATLAB/SIMULINK, and its performance is analyzed with experimental results. These results show that the new Z-source propulsion system has a promising application in new energy ships, as it has higher reliability and lower complexity and cost compared to conventional propulsion systems.

Keywords: hybrid power; ship; electrical propulsion; Z-source inverter; ship grid impulse

Citation: Gan, S.; Shi, W.; Xu, X. Proposed Z-Source Electrical Propulsion System of a Fuel Cell/Supercapacitor-Powered Ship. *J. Mar. Sci. Eng.* **2023**, *11*, 1543. https://doi.org/10.3390/jmse11081543

Academic Editors: Alon Gany and Leszek Chybowski

Received: 14 June 2023
Revised: 30 July 2023
Accepted: 31 July 2023
Published: 2 August 2023

1. Introduction

With the growing global concern about energy saving and emission reduction, more and more scholars and ship manufacturers are focusing on new energy ships [1–3] and advanced propulsion systems [4–6]. The electric propulsion ship is more reliable and versatile than conventional mechanical propulsion ships. Furthermore, the electric propulsion ship has an additional advantage of possible cost reduction due to fewer prime movers and greater fuel savings [5,7].

Electric propulsion is an advanced ship propulsion method, and it uses the motor to drive the propeller. Its core is the propulsion inverter. However, conventional propulsion inverters have no simultaneous buck–boost conversion capabilities. They are either a boost or a buck converter and cannot be a buck–boost converter. That is, the output voltage is either greater or smaller than the input voltage. To overcome the above shortcomings, Peng [8] proposed a single-stage Z-source inverter with a buck–boost conversion capability. It is very suitable for new energy power generation occasions where the voltage fluctuation is relatively large. The Z-source inverter has an important application value in the fields of electric vehicles and ships [9–12], new energy power generation [13–15], and motor drive [16–18].

Among different green energy sources, FCs have gained global attention. Now it is used more and more in electric transportation equipment. However, due to the low

dynamic reaction of the FCs, batteries or SCs are incorporated to accelerate the energy system response [19–22]. As with other microgrids, optimizing the different energy sources on board is one of the main concerns of ship operations. Considering the cost, reliability issues, and different operational constraints, the energy management system should utilize rechargeable devices and batteries to maintain a balance between supply and demand throughout the sailing period. Optimal methods of energy resources for ships have been extensively studied in the literature. These studies have used different optimization methods, such as classical optimization [22–24], dynamic programming [25,26], and rule-based methods [27,28], to solve energy management problems. In [25], the optimal energy management of an emission-free ship is studied. FCs are considered the main energy resource for supplying the loads, and batteries are considered auxiliary energy resources for covering fast demand fluctuations.

In order to reduce ship emissions and maintain the operation security of the ship microgrid, a proposed HVB-ZSI is used in the propulsion system of a hybrid inland river cruise ship. The operating modes and control strategy of the hybrid power electrical propulsion system with a fuel cell (FC) as the main power source and supercapacitor (SC) as the auxiliary power source are studied in detail. Since the inland river cruise ship is frequently operated in the starting and braking state, SCs are chosen as the energy storage device instead of batteries in this study to balance the difference between the two powers and to absorb the regenerative braking energy. The FC delivers average power for the propulsion system, and the SC delivers dynamic power. At the same time, the SC absorbs the excess power of the FC and regenerative braking energy. This paper presents the control strategy and demonstrates these features for use in a hybrid cruise ship. The performance is validated by both simulated and experimental results.

Compared to [25], the SC has a quicker response, better safety, and longer life than batteries. Because the propulsion system adopts the proposed HVB-ZSI, it is very adaptable to the disadvantage that the FC output voltage fluctuates greatly.

The proposed propulsion system can improve the ship's efficiency and reduce the cost due to a lower power switch count since it is a one-stage converter with a reduced volume and an easier control algorithm. It reduces line harmonics, Z-source capacitor voltage stress, and current surge limitation at startup, improves power factor and reliability, and extends the output voltage range [29].

2. Configuration and Operation Modes of the Hybrid Ship

The power inverter is the key component in the ship's propulsion system for handling all power flow. The proposed HVB-ZSI [29] is used to replace the two-stage power conversion in the hybrid power ship, as shown in Figure 1. The proposed HVB-ZSI supplies the requested power to the traction motor and absorbs regenerative braking energy. Vector control technology is used to control the speed of the traction motor during motoring and regenerative braking operations.

In Figure 1, SVPWM is the space vector pulse-width modulation. From Figure 1, it can be seen that the system control includes two parts: the DC-side capacitor voltage closed-loop control and the AC-side speed control. The DC-side capacitor voltage control generates a shoot-through signal D, and the AC-side speed control generates a modulation ratio M according to the operating state of the hybrid power ship. Thus, the output power of the FC and SC is controlled.

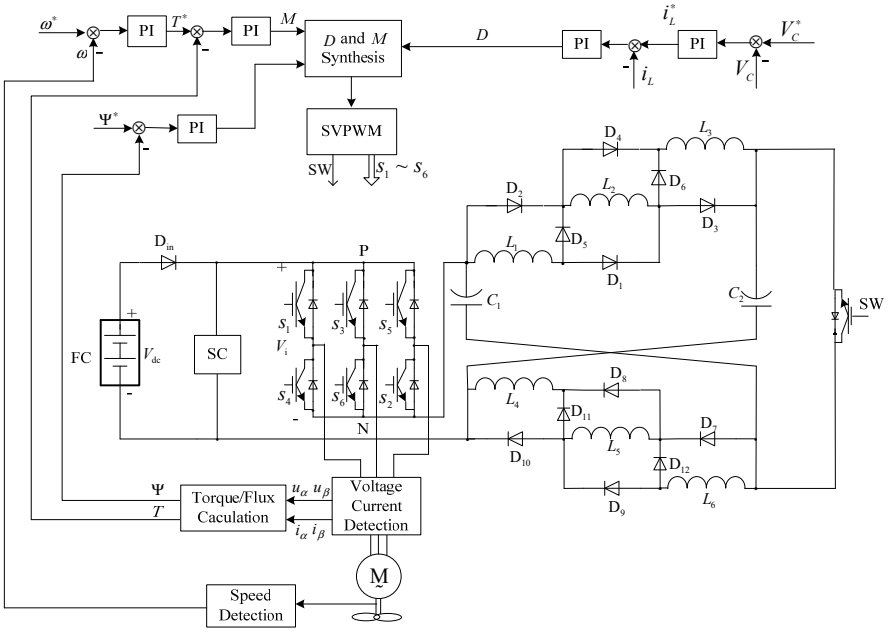

Figure 1. Proposed Z-source propulsion system.

The hybrid ship is powered by two energy sources. The main energy source is an FC. The auxiliary energy source is an SC, which also stores excess energy from the FC or regenerative braking energy of the traction motor. The ship has four operating modes, and the four modes of operation are described as follows:

① Mode 1: When the power demanded by the ship is moderate, the propulsion motor is powered by FC, and if the state of charge (SOC) of the SC, SOC < SCO_H, the FC also charges the SC, as shown in Figure 2.

② Mode 2: When the ship is accelerated or overloaded, the FC and SC work together to power the propulsion system. The SC provides dynamic power to accelerate the ship's response speed or overload power, while the FC provides steady-state power. The power flow is shown in Figure 2.

③ Mode 3: When the ship is braked to slow down, the regenerative braking energy is stored back into the SC. The power flow in the mode is shown in Figure 2.

④ Mode 4: When the ship is sailing at a low speed, and the power demand is very small, the SC supplies power to the ship alone, and the FC also charges the SC. The power flow in the mode is shown in Figure 2.

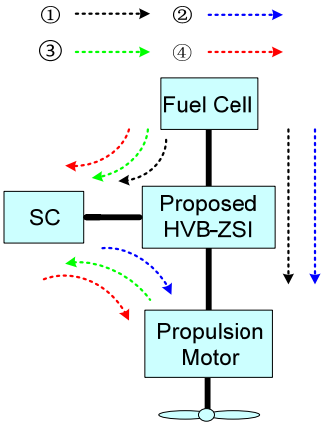

Figure 2. Energy flow schematics in different modes.

3. Principle of the Proposed HVB-ZSI System

The circuit components of the proposed HVB-ZSI, as shown in Figure 1, are almost the same as those of the HVB-ZSI [30]. The difference is that the positions of the inverter and Z-source network are swapped, and their connection direction is reversed, which can suppress the inrush current during starting and avoid inverter damage. The second difference is that the active switch SW is added, and the current of the proposed Z-source circuit can flow in the opposite direction; thus, the quality of the inverter output voltage is improved.

Assuming that the Z-source circuit is symmetric, that is, $C_1 = C_2$, $L_1 = L_2 = L_3 = L_4 = L_5 = L_6$, so

$$u_{L1} = u_{L2} = u_{L3} = u_{L4} = u_{L5} = u_{L6} = u_L,\ V_{C1} = V_{C2} = V_C \tag{1}$$

For simplicity, the Z-source equivalent circuit viewed from the inverter side is shown in Figure 3. In Figure 3, R_0 is the equivalent resistance, and L_0 is the motor equivalent inductor converted to the DC side. From the power balance, $R_0 = 8\,|\,Z_{ac}\,|\,/3cos\varphi$. $cos\varphi$ is the motor power factor, and Z_{ac} is the motor per phase impedance; $Z_{ac} = R_{ac} + jL_{ac}$ [31]. The inverter shown in Figure 1 can be simplified into two operating states: the shoot-through state and the non-shoot-through state. When the inverter is working in the shoot-through state, as shown in Figure 3a, Equation (2) can be obtained from Figure 3a:

$$\begin{aligned} V_L &= V_{\mathrm{dc}} + V_{\mathrm{C}} \\ V_i &= 0 \end{aligned} \tag{2}$$

where V_L is the inductance voltage, V_C is the capacitor voltage, V_{dc} is the input DC voltage, and V_i is the DC-link voltage.

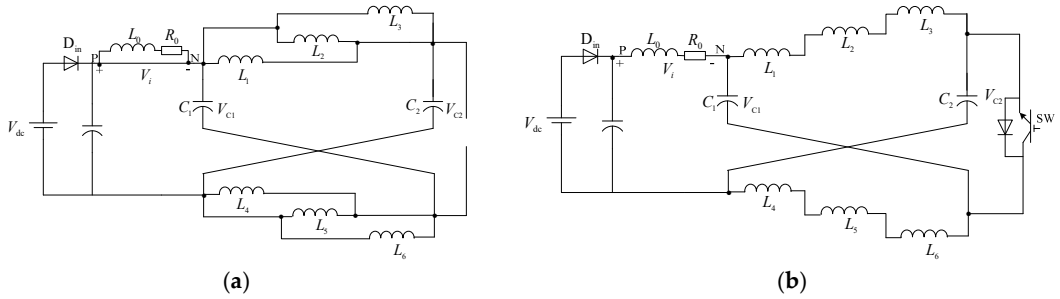

Figure 3. Equivalent circuits. (**a**) Shoot-through and (**b**) Non-shoot-through.

The equivalent circuit of the non-shoot-through state is shown in Figure 3b. In this state, the diode D_{in} is on, and the energy stored in the inductors is fed back to the inverter. From Figure 3b, the equation can be expressed as follows:

$$\begin{aligned} 3V_{\mathrm{L}} &= -V_{\mathrm{C}} \\ V_i &= V_{\mathrm{dc}} + V_{\mathrm{C}} - 3V_{\mathrm{L}} \end{aligned} \tag{3}$$

In a cycle, the average voltage across the inductance is equal to 0, then

$$T_0 V_C + \frac{(V_i - V_{\mathrm{C}})}{3}(T - T_0) = 0 \tag{4}$$

Assuming that the shoot-through duty ratio is $D = T_0/T$, according to Equation (4), the capacitor voltage can be derived as follows:

$$V_{\mathrm{C}} = \frac{3D}{1 - 4D} V_{\mathrm{dc}} \tag{5}$$

The peak DC-link voltage across the inverter bridge can be expressed as

$$V_{\mathrm{i}} = \frac{1+2D}{1-4D} V_{\mathrm{dc}} = BV_{\mathrm{dc}} \tag{6}$$

where B is the boost factor.

The boost factors of the conventional ZSI and HVB-ZSI are given in [7,24]. The B comparison of the three inverters is shown in Figure 4. From Figure 4, it can be seen that under the same D, the proposed HVB-ZSI has the same boost capacity as HVB-ZSI, but it is much higher than the conventional ZSI.

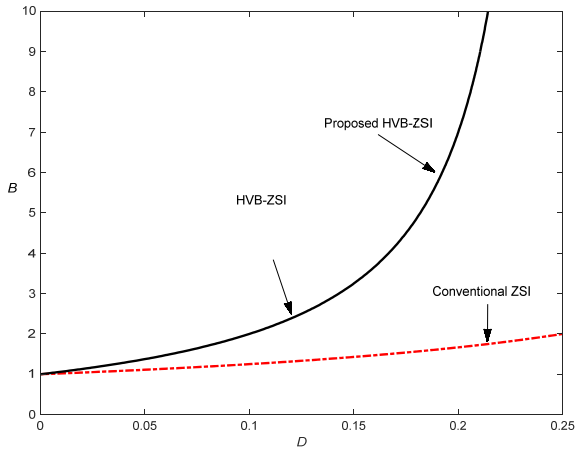

Figure 4. B vs. D of the three topologies.

The output voltage of the inverter is expressed as follows:

$$V_{\mathbf{o}} = \frac{\mathbf{1}}{\mathbf{2}} BMV_i \tag{7}$$

Compared with HVB-ZSI, the proposed HVB-VSI has the advantages of lower Z-source capacitor voltage stress and smaller surge current at startup. By employing an input capacitor and an active switch, the current of the Z-source network flows in the reverse direction, thus making the inverter more suitable for applications where the load current varies widely [29].

4. Modeling and Control Strategy of the Propulsion System

4.1. Capacitor Voltage Control of the DC Side

By selecting the capacitor voltage u_c, inductance current i_L, and inverter output current i_0 as state variables, the average state equation of the proposed Z-source circuit is derived as follows:

$$\frac{d}{dt}\begin{pmatrix} i_L \\ v_C \\ i_0 \end{pmatrix} = \begin{pmatrix} 0 & \frac{4d-1}{3L} & 0 \\ \frac{1-4d}{C} & 0 & -\frac{m}{C} \\ 0 & \frac{2m}{L0} & -\frac{R0}{L0} \end{pmatrix} \begin{pmatrix} i_L \\ v_C \\ i_0 \end{pmatrix} + \begin{pmatrix} \frac{d}{L} v_{\mathrm{dc}} \\ 0 \\ \frac{V_{\mathrm{dc}}}{L0} m \end{pmatrix} \tag{8}$$

Given that the state variable is the sum of the static component and small-signal component, that is

$$\begin{cases} v_C = V_C + \hat{v}_C \\ i_L = I_L + \hat{i}_L \\ i_{\mathbf{0}} = I_{\mathbf{0}} + \hat{i}_{\mathbf{0}} \\ v_{\mathrm{dc}} = V_{\mathrm{dc}} + \hat{v}_{\mathrm{dc}} \\ d = D + \hat{d} \end{cases} \tag{9}$$

Substituting Equation (9) into (8), the small-signal model equation can be derived as follows:

$$\frac{d}{dt}\begin{pmatrix}\hat{i}_L\\ \hat{v}_C\\ \hat{i}_0\end{pmatrix}=\begin{pmatrix}0 & \frac{4[D+\hat{d}(t)]-1}{3L} & 0\\ \frac{1-4[D+\hat{d}(t)]}{C} & 0 & -\frac{M+\hat{m}(t)}{C}\\ 0 & \frac{2[M+\hat{m}(t)]}{L_0} & \frac{-R_0}{L_0}\end{pmatrix}\begin{pmatrix}I_L+\hat{i}_L(t)\\ V_C+\hat{v}_C(t)\\ I_0+\hat{i}_0(t)\end{pmatrix}+\begin{pmatrix}\frac{D+\hat{d}}{L}\\ 0\\ \frac{M+\hat{m}(t)}{L_0}\end{pmatrix}(V_{dc}+\hat{v}_{dc}(t)) \tag{10}$$

From Equation (10), the transfer function $G_{ud}(s)$ of the capacitor voltage to the shoot-through duty ratio can be derived as

$$G_{ud}=\frac{\hat{v}_C}{\hat{d}}=\frac{3(sL_0+R)\cdot[(4V_C+3V_{dc})(1-4D)-4sLI_L]}{3s^3CLL_0+3s^2CLR_0+[(1-4D)^2L_0+6M^2L]s+(1-2D)^2R_0} \tag{11}$$

The transfer function $G_{id}(s)$ of the inductance current to the shoot-through duty ratio can be obtained as

$$G_{id}=\frac{\hat{i}_L}{\hat{d}}=\frac{(4V_C+3V_{dc})CL_0s^2+[(4V_C+3V_{dc})CR_0+4(1-4D)I_LL_0]s-4(4D-1)I_LR_0+2M^2((4V_c+3V_{dc})}{3s^3CLL_0+3s^2CLR_0+[(1-4D)^2L_0+6M^2L]s+(1-2D)^2R_0} \tag{12}$$

The DC-link voltage directly affects the stability of the AC-side output voltage. Using a single-loop voltage control, the inductance current of the Z-source can not be effectively controlled. And thus, a double-loop control is used to overcome the above problem in this study [28]. However, owing to the existence of the shoot-through zero vector, it is difficult to detect and feed back the DC-link voltage, so the DC-link voltage is controlled indirectly through the capacitor voltage V_c of the Z-source. The double-loop control is shown in Figure 5.

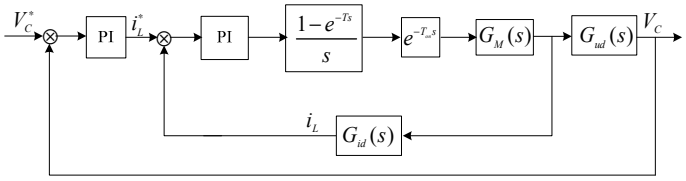

Figure 5. Double-loop control.

In Figure 5, $G_{ud}(s)$ and $G_{id}(s)$ are shown in Equations (11) and (12), respectively. $\frac{1-e^{-Ts}}{s}$ is the zero-order holder, T is the sampling period, $e^{-T_{on}s}$ is the calculating delay link, and the delay time T_{on} is half of T. G_M (s) is the transfer function of the shoot-through duty cycle to the modulation signal, which is expressed as [31]

$$G_M(s)=\frac{D(s)}{v_m(s)}=\frac{2}{V_{tri}} \tag{13}$$

where V_{tri} is the carrier signal amplitude.

When the current loop has a 1 kHz crossover frequency according to the simulation parameters in Section 5, the phase margin is 64°. The voltage loop has a 130 Hz crossover frequency and 68° phase margin.

4.2. Propulsion Motor Control of the AC Side

The modulation signals are generated by the AC-side controller, as shown in Figure 1. When the ship is sailing at low speed, the Z-source inverter works in the low-frequency region, and the demanded voltage of the propulsion motor is also very low. Therefore, the DC-link voltage does not need to be boosted, and the Z-source inverter does not work in the shoot-through state. The voltage of the propulsion motor is gradually increased by adjusting the modulation factor M. When the ship is sailing at high speed, the Z-source inverter works in the high-frequency region. Because the DC-link voltage is not sufficient to

generate the desired AC voltage, a shoot-through signal is introduced. The shoot-through signal generated on the DC side and the SPWM signal generated on the AC side are combined and sent to a trigger circuit to drive the propulsion motor.

4.3. Control Strategy of SW

According to the analysis [29], the active switch SW provides a reverse path for the reverse current so that the output current meets the load current requirement. The driving signal of switch SW is opposite to that of the shoot-through signal. This way, the DC-link voltage is not distorted in all working states, thus eliminating the problem of DC-link voltage distortion under abnormal working conditions with relatively low loads or small inductance.

4.4. Energy Control Strategy

When a hybrid ship is sailing, it switches between the above four operating modes. However, no matter which mode it is operating in, when SOC < SOC_L, the energy controller forces the SC to enter the charging mode and prohibits it from continuing to discharge. When SOC > SCO_H, the SC cannot continue to store regenerative braking energy, and the braking energy is consumed by the resistor.

The demand power of the traction motor changes at any time. The output voltage of FC is highly dependent on the output current. Therefore, the FC voltage is controlled by Equation (5) for a given capacitor voltage. So, the output current and power of the FC is determined by its V-I characteristic. The output power of the FC is expressed as follows:

$$P_{FC} = V_{FC} I_{FC} \tag{14}$$

At the same time, the desired output voltage V_o of the Z-source inverter is obtained by controlling D and M, as shown in Equation (7). Therefore, the inverter output power is expressed as

$$P_o = \frac{3}{\sqrt{2}} V_o I_o cos\varphi \tag{15}$$

where I_o is the load current and $cos\varphi$ is the load power factor.

Because the system can control the output power of the FC and inverter, the power of the SC satisfies the following Equation:

$$P_{SC} = P_o - P_{FC} \tag{16}$$

5. Simulation and Experiment

5.1. Simulation Results

To verify the above-mentioned principle and the control strategy, the simulation model shown in Figure 1 is established using the MATLAB/Simulink platform. The proposed HVB-ZSI adopts a simple boost-control method. The simulation parameters are as follows:

(1) Z-source circuit: $L_1 = L_2 = L_3 = L_4 = L_5 = L_6 = 0.5$ mH, $C_1 = C_2 = 1200$ μF;
(2) Output filters: $L_f = 1500$ μH, $C_f = 20$ μF;
(3) Load: R = 15 Ω/phase;
(4) Switching frequency: 20 kHz.

Case 1: $V_{dc} = 100$ V, $D = 0.1926$, $M = 0.807$. From the aforementioned equations, $B = 6.022$, $G = 4.863$, $V_C = 251.1$ V, and $V_i = 602.2$ V.

The simulation results of the proposed inverter are shown in Figure 6a. In Figure 6, the curves from top to bottom are the DC-link voltage V_i, capacitor voltage V_C, output voltage V_o, and inductance current i_L. From Figure 6a, it can be seen that the capacitor voltage V_C is boosted to 249 V, V_i is boosted to 602 V, and the Z-source inductance inrush current is greatly reduced.

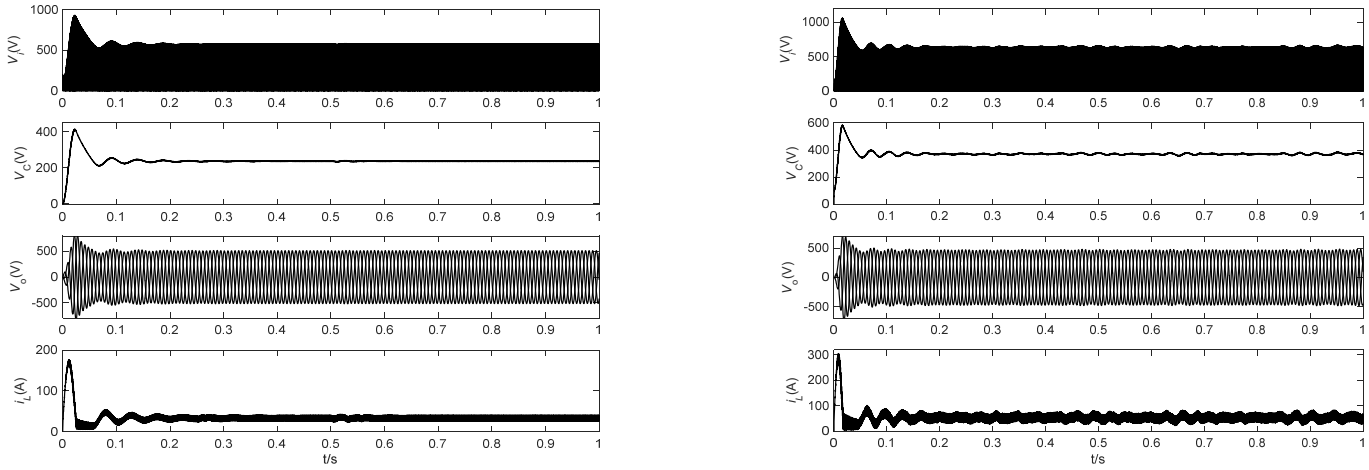

(**a**) (**b**)

Figure 6. Simulation results in case 1. (**a**) Proposed HVB-ZSI; (**b**) HVB-ZSI.

The simulation results of the HVB-ZSI are shown in Figure 6b. From Figure 6b, we can see that V_C is boosted to 383 V, V_i is boosted to 602 V, and the inrush current is very large when starting, which may damage the inverter.

Figure 7 shows the V_i and i_L waveforms of the two inverters at light load (R = 300 Ω/phase). From Figure 7, it can be seen that the proposed HVB-ZSI can eliminate the DC-link voltage distortion in the light-load state. The simulation results confirm the correctness of the above analysis.

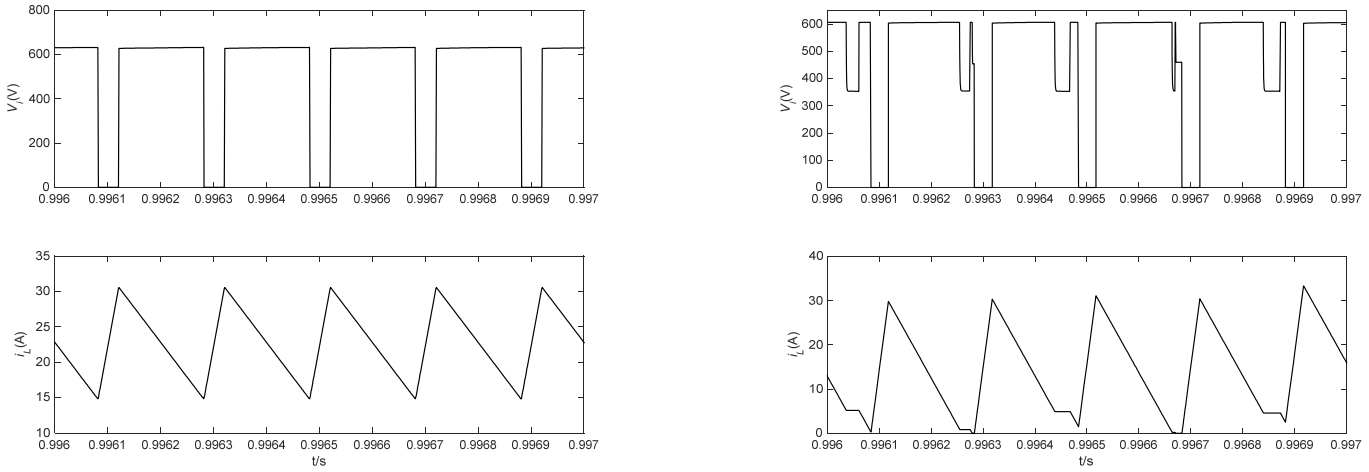

(**a**) (**b**)

Figure 7. DC-link voltage and inductor current at light load. (**a**) Proposed HVB-ZSI; (**b**) HVB-ZSI.

Case 2: Assuming that the input voltage V_{dc} of the proposed HVB-ZSI suddenly drops from 120 V to 100 V, the simulation results are shown in Figure 8. In Figure 8, the curves from top to bottom are the input voltage V_{dc}, DC-link voltage V_i, capacitor voltage V_C, output voltage V_o, and shoot-through duty cycle D. In order to maintain a stable output voltage, the shoot-through duty cycle D rises, which makes the capacitor voltage rise to compensate for the input voltage drop.

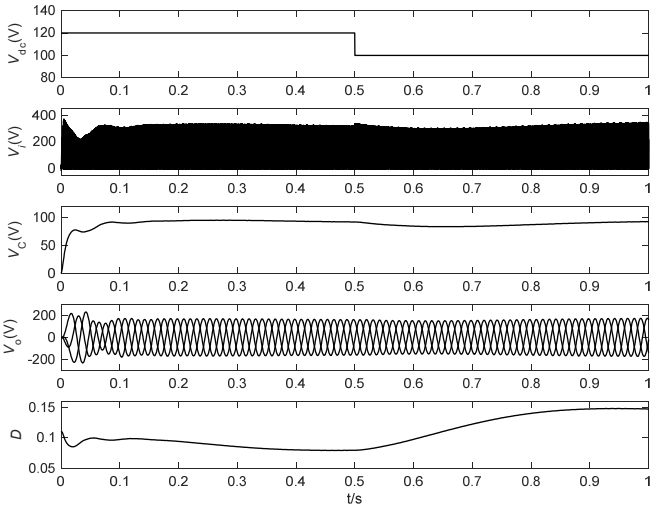

Figure 8. Simulation results in case 2.

In electric propulsion ships, the propeller is driven directly by the propulsion motor, and the propeller load torque can be simplified as follows:

$$T_L = K_M \rho D_{ia}^5 n^2 = K n^2 \tag{17}$$

where K_M is the torque coefficient, ρ is the water density, D_{ia} is the propeller diameter, and n is the propeller speed.

The simulation does not consider other factors but only considers the relationship between propeller torque and speed.

To further confirm the control strategy of the hybrid ship in different operating modes, a dynamic simulation model is built, and the simulation parameters are shown in Table 1.

Table 1. Parameters of the hybrid ship.

Ship parameter	**Value**
Type	Passenger
Overall length (m)	5.8
Beam(m)	2.08
Maximum speed(knots)	10
Average speed(knots)	8
Motor parameter	**Value**
Type	IM
Rated power(kW)	3
FC parameter	**Value**
Power [Min, Max]/kW	[2, 5]
Voltage [Min, Max]/V	[150, 225]
SC parameter	**Value**
Rated capacitance(mF)	145
Rated voltage	208 V

In the simulation, the real-time torque of the propeller is used as the load torque of the propulsion motor. Figure 9 shows the simulation results.

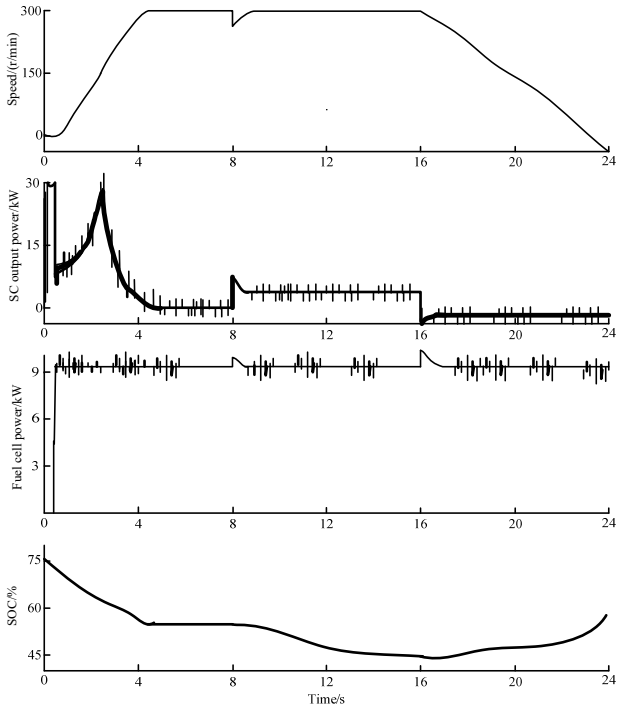

Figure 9. Curves of motor speed, fuel cell power, super capacitor power and SOC.

In Figure 9, the curves from top to bottom are the propulsion motor speed n, output power of the SC, output power of FC, and SOC. ① Stage 1 (0–5 s): in this stage, the ship starts and accelerates from 0 to 300 r/min with the rated load, and the ship sails in mode 2; ② Stage 2 (5–8 s): The ship sails at a constant speed with rated load, and during this phase, the ship operates in mode 1; ③ Stage 3 (8–16 s): at 8 s, the ship sails at 1.2 T_N; ④ Stage 4 (16–24 s): In this phase, the ship brakes and works in the regenerative braking state, and the regenerative braking energy is stored into the SC. As seen in Figure 9, the average power is delivered by the FC and the dynamic power is supplied by the SC in stage 1; the SOC of SC gradually decreases, and the hybrid power ship runs in mode 2. In stage 2, the ship sails at a constant speed in mode 1; the rated power is delivered by the FC, the SC does not deliver the power, and the SOC does not change. In stage 3, the ship is overloaded, the FC delivers the rated power, and the SC delivers the overload power; the hybrid power ship runs in mode 2. In stage 4, the ship brakes to a stop, the SC absorbs the regenerative braking energy, and the hybrid power ship operates in mode 3; the SOC gradually increases.

The simulation curves of the ship's staged startup are shown in Figure 10. From top to bottom, the curves are the DC-side voltage V_i, output line voltage V_{AB} of the inverter, capacitor voltage V_C, inductance current i_L, speed n, electromagnetic torque T_e, and propeller load torque T_L. The given speed of the propulsion motor is set to 100 r/min from 0 to 0.5 s, 200 r/min from 0.5 s to 1 s and 290 r/min from 1 s to 1.5 s. Regardless of other factors, propeller speed quickly tracks to the given speed.

From Figure 10, it can be seen that the given speed increases from 100 rpm to 200 rpm at 0.5 s. As the speed increases, the torque of the propeller also increases from 15 N.m to 25 N·m. After a short period of adjustment, the electromagnetic torque of the propulsion motor also increases to 25 N·m. At 1 s, the given speed of the propulsion motor increases from 200 r/min to 290 r/min. The propeller torque and electromagnetic torque also increase.

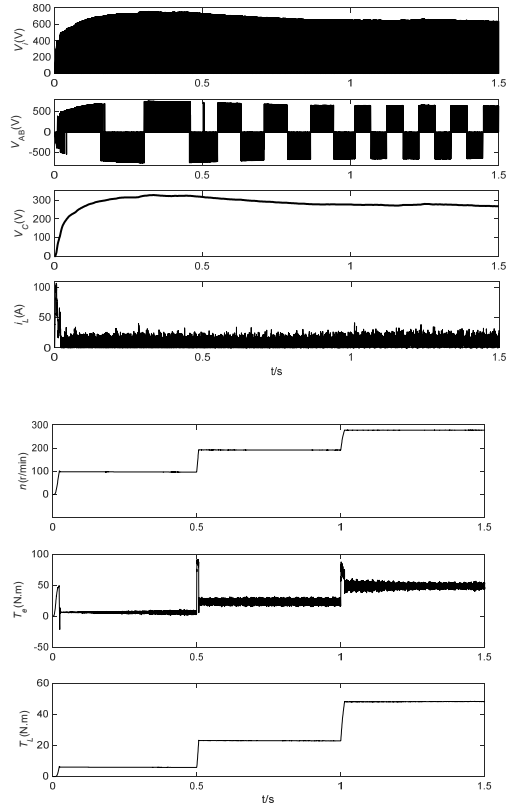

Figure 10. Simulation results of the ship's staged startup.

5.2. Experimental Results

To confirm the above principle and simulation, a hardware prototype of the proposed HVB-ZSI, as shown in Figure 11, was built. The circuit parameters are $L_1 = L_2 = L_3 = L_4 = L_5 = L_6 = 0.5$ mH, and $C_1 = C_2 = 1200$ μF. The rated capacity of the SC is 415 mF, and the rated voltage is 208 V. The output power of the FC in normal operation ranges from 6 kw to 10 kw, and the output voltage ranges from 150 V to 225 V. The switching frequency is 20 kHz.

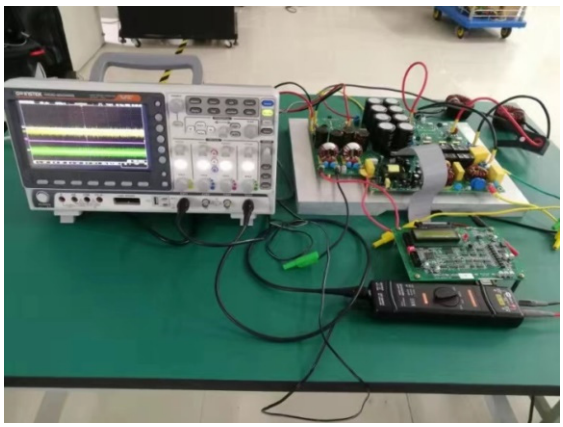

Figure 11. Experimental circuit.

The experimental curves of the proposed HVB-ZSI in case 1 are shown in Figure 12. As shown in Figure 12, V_C is boosted to 252 V, V_i is boosted to 598 V, and the peak value of phase voltage u_a is 311 V. The experimental results are almost the same as those of the simulation results.

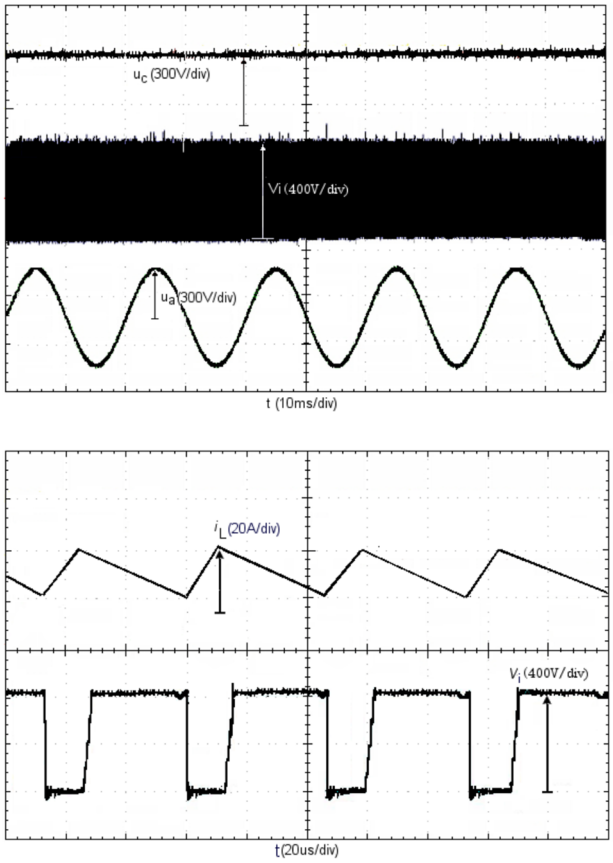

Figure 12. Experimental waveforms.

A hybrid inland river cruise ship based on the proposed HVB-ZSI was built in the laboratory, as shown in Figure 13. The type of the ship is a passenger ship, the length is 5.8 m, and the width is 2.08 m. The rated power of the propulsion AC asynchronous motor is 7.5 kw, and the average speed is 8 knots. The inland river cruise ship is supplied by an FC as the main power source and an SC as the auxiliary power source. The hybrid inland river cruise ship parameters are shown in Table 1.

Figure 13. Hybrid power ship.

The ship started with a rated load of 2 s and sailed for a period of time, then suddenly increased the 20% rated load at 20 s. The ship braked at 30 s, and after 40 s, the ship sailed at a very low speed. The experimental results are shown in Figure 14, which are basically the same as Figure 9.

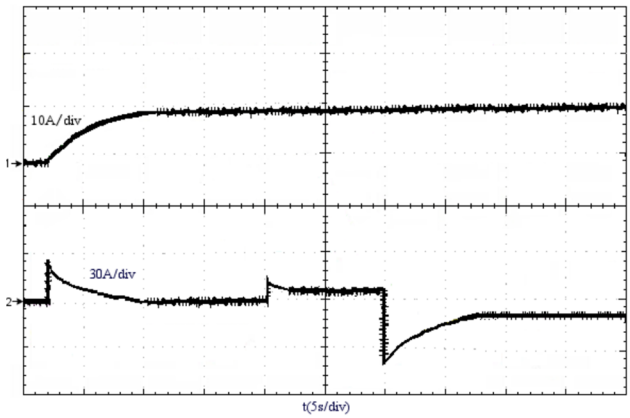

Figure 14. Current waveforms of FC and SC.

In Figure 14, the upper curve is the output current of the FC, and the lower curve is the SC output current. When the ship starts at 2 s, the output current of the FC gradually increases, and its accelerating dynamic current is provided by the SC; the hybrid ship sails in mode 2. When the ship runs at a constant speed with a rated load, the FC provides the rated current, and the SC does not provide the current; the ship operates in mode 1. Between 20 and 30 s, the ship overloads. The FC provides the rated current, and the remaining current is supplied by the SC, which works in mode 2. When the ship brakes at 30 s, the regenerative braking energy is stored into the SC; the system runs in mode 3. After 40 s, the ship cruises at low speed. The FC powers the ship and simultaneously charges the SC; the system runs in mode 3. The experimental results verify the principles and simulations.

6. Conclusions

In this paper, an FC/SC-powered ship based on the proposed HVB-ZSI was studied. This proposed HVB-ZSI has good prospects for application in electric propulsion ships because of the following merits: (1) The propulsion system has high-voltage-boost ability and is well suited for use in FC power systems; (2) the Z-source capacitor voltage stress is reduced greatly under the same boost ability, and the inrush current can be suppressed; (3) the proposed propulsion system can improve the ship efficiency and reduce the cost due to a lower power switch count; and (4) no DC-DC converter is needed to control the SOC of the SC, as the power of the hybrid energy source can be controlled by a straight-through duty cycle and modulation factor. The operating modes and control strategy of using the proposed HVB-ZSI for an FC/SC-powered ship are discussed in this paper and confirmed by simulation and experimental results.

In the future, we will continue to study the optimal matching of the two energy capacities and optimal energy control.

Author Contributions: Conceptualization and methodology, S.G.; software, S.G. and W.S.; validation, X.X.; formal analysis, S.G.; investigation, X.X.; writing—original draft preparation, S.G. and W.S.; writing—review and editing, X.X.; visualization, X.X.; supervision, S.G. All authors have read and agreed to the published version of the manuscript.

Funding: This research was funded by [The Shanghai Science and Technology Commission project], grant number [20040501200, 19040501700]; and by [The Science & Technology Commission of Shanghai Municipality and Shanghai Engineering Research Center of Ship Intelligent Maintenance and Energy Efficiency], grant number [20DZ2252300].

Institutional Review Board Statement: Not applicable.

Informed Consent Statement: Not applicable.

Data Availability Statement: The data supporting the reported results cannot be shared at this time, as it has been used in producing more publications on this research.

Acknowledgments: This work was supported by the Shanghai Science and Technology Commission project (Grant No. 20040501200, 19040501700) and the Science & Technology Commission of Shanghai Municipality and Shanghai Engineering Research Center of Ship Intelligent Maintenance and Energy Efficiency project (Grant No.20DZ2252300).

Conflicts of Interest: The authors declare no conflict of interest.

References

1. Wen, S.; Zhang, C.; Lan, H.; Xu, Y.; Tang, Y.; Huang, Y. A Hybrid ensemble model for interval prediction of solar power output in ship onboard power Systems. *IEEE Trans. Sustain. Energy* **2021**, *12*, 14–24. [CrossRef]
2. Bucci, V.; Marinò, A.; Bosich, D.; Sulligoi, G. Inland waterway gas-fueled vessels: CASM-based electrification of a pushboat for the european network. *IEEE Trans. Transp. Electrif.* **2016**, *2*, 607–617. [CrossRef]
3. Kim, K.; Park, K.; Lee, J.; Chun, K.; Lee, S.H. Analysis of battery/generator hybrid container ship for CO_2 reduction. *IEEE Access* **2018**, *6*, 14537–14545. [CrossRef]
4. Xu, X.; Song, X.; Wang, K.; Liu, N.; Long, W.; Zheng, Z.; Li, Y. Modulation and voltage balancing control of dual five-level ANPC inverter for ship electric propulsion systems. *Chin. J. Electr. Eng.* **2021**, *7*, 78–92. [CrossRef]
5. Ghimire, P.; Zadeh, M.; Thorstensen, J.; Pedersen, E. Data-driven efficiency modeling and analysis of all-Electric ship powertrain: A comparison of power system architectures. *IEEE Trans. Transp. Electrif.* **2022**, *8*, 1930–1943. [CrossRef]
6. Sulligoi, G.; Vicenzutti, A.; Menis, R. All-electric ship design: From electrical propulsion to integrated electrical and electronic power systems. *IEEE Trans. Transp. Electrif.* **2016**, *2*, 507–521. [CrossRef]
7. Reusser, C.A.; Young, H.A.; Osses, J.R.P.; Perez, M.A.; Simmonds, O.J. Power electronics and drives: Applications to modern ship propulsion systems. *IEEE Ind. Electron. Mag.* **2020**, *14*, 106–122. [CrossRef]
8. Peng, F.Z. Z-source inverter. *IEEE Trans. Ind. Appl.* **2003**, *39*, 504–510. [CrossRef]
9. Battiston, A.; Miliani, E.H.; Pierfederici, S.; Meibody-Tabar, F. Efficiency improvement of a quasi-Z-source inverter-fed permanent-magnet synchronous machine-based electric vehicle. *IEEE Trans. Transp. Electrif.* **2016**, *2*, 14–23. [CrossRef]
10. Hu, S.; Liang, Z.; Fan, D.; He, X. Hybrid ultracapacitor–battery energy storage system based on quasi-Z-source topology and enhanced frequency dividing coordinated control for EV. *IEEE Trans. Power Electron.* **2016**, *31*, 7598–7610. [CrossRef]
11. Nie, Z. The development of new-style photovoltaic Z-source inverter of ship. In Proceedings of the IEEE 2012 Power Engineering and Automation Conference, Wuhan, China, 18–20 September 2012.
12. Sonandkar, S.; Selvaraj, R.; Chelliah, T.R. Fault tolerant capability of battery assisted quasi-Z-source inverter fed five phase PMSM drive for marine propulsion applications. In Proceedings of the 2020 IEEE International Conference on Power Electronics, Drives and Energy Systems (PEDES), Jaipur, India, 16–19 December 2020.
13. Singh, S.A.; Carli, G.; Azeez, N.A.; Williamson, S.S. Modeling, design, control, and implementation of a modified Z-source integrated PV/grid/EV DC charger/inverter. *IEEE Trans. Ind. Electron.* **2018**, *65*, 5213–5220. [CrossRef]
14. Ge, B.; Liu, Y.; Abu-Rub, H.; Peng, F.Z. State-of-charge balancing control for a battery-energy-stored quasi-Z-source cascaded-multilevel-inverter-based photovoltaic power System. *IEEE Trans. Ind. Electron.* **2018**, *65*, 2268–2279. [CrossRef]
15. Liang, W.; Liu, Y.; Peng, J. A day and night operational quasi-Z source multilevel grid-tied PV power system to achieve active and reactive power control. *IEEE Trans. Power Electron.* **2021**, *36*, 474–492. [CrossRef]
16. Li, X.; Xia, C.; Cao, Y.; Chen, W.; Shi, T. Commutation torque ripple reduction strategy of Z-source inverter fed brushless DC motor. *IEEE Trans. Power Electron.* **2016**, *31*, 7677–7690. [CrossRef]
17. Xiao, S.; Shi, T.; Li, X.; Wang, Z.; Xia, C. Single-current-sensor control for PMSM driven by quasi-Z-source inverter. *IEEE Trans. Power Electron.* **2019**, *34*, 7013–7024. [CrossRef]
18. Mahmoudi, H.; Aleenejad, M.; Ahmadi, R. Torque ripple minimization for a permanent magnet synchronous motor using a modified quasi-Z-source inverter. *IEEE Trans. Power Electron.* **2019**, *34*, 3819–3830. [CrossRef]
19. Meng, X.; Li, Q.; Zhang, G.; Wang, T.; Chen, W.; Cao, T. A dual-mode Energy management strategy considering fuel cell degradation for energy consumption and fuel cell efficiency comprehensive optimization of hybrid vehicle. *IEEE Access* **2019**, *7*, 134475–134487. [CrossRef]
20. Zendegan, S.; Ferrara, A.; Jakubek, S.; Hametner, C. Predictive battery state of charge reference generation using basic route information for optimal energy management of heavy-duty fuel cell vehicles. *IEEE Trans. Veh. Technol.* **2021**, *70*, 12517–12528. [CrossRef]
21. Shen, D.; Lim, C.C.; Shi, P. Fuzzy model based control for energy management and optimization in fuel cell vehicles. *IEEE Trans. Veh. Technol.* **2020**, *69*, 14674–14688. [CrossRef]
22. Zhang, Z.; Guan, C.; Liu, Z. Real-time optimization energy management strategy for fuel cell hybrid ships considering power sources degradation. *IEEE Access* **2020**, *8*, 87046–87059. [CrossRef]
23. He, L.; Li, Y.; Shuai, Z.; Guerrero, J.M.; Cao, Y.; Wen, M.; Shi, J. A flexible power control strategy for hybrid AC/DC zones of shipboard power system with distributed energy storages. *IEEE Trans. Ind. Inform.* **2018**, *14*, 5496–5508. [CrossRef]
24. Balsamo, F.; Capasso, C.; Miccione, G.; Veneri, O. Hybrid Storage System Control Strategy for All-Electric Powered Ships. *Energy Procedia* **2017**, *126*, 1083–1090. [CrossRef]

25. Banaei, M.; Rafiei, M.; Boudjadar, J.; Khooban, M.H. A comparative analysis of optimal operation scenarios in hybrid emission-free ferry ships. *IEEE Trans. Transp. Electrif.* **2020**, *6*, 318–333. [CrossRef]
26. Kanellos, F.D.; Tsekouras, G.J.; Hatziargyriou, N.D. Optimal demand-side management and power generation scheduling in an all-electric ship. *IEEE Trans. Sustain. Energy* **2014**, *5*, 1166–1175. [CrossRef]
27. Rafiei, M.; Boudjadar, J.; Khooban, M.H. Energy management of a zero-emission ferry boat with a fuel-cell-based hybrid energy system: Feasibility assessment. *IEEE Trans. Ind. Electron.* **2021**, *68*, 1739–1748. [CrossRef]
28. Han, J.; Charpentier, J.F.; Tang, T. An energy management system of a fuel cell/battery hybrid boat. *Energies* **2014**, *7*, 2799–2820. [CrossRef]
29. Gan, S.; Shi, W. An improved Z-source inverter with high voltage boost ability. *Electr. Eng.* **2021**, *104*, 869–881. [CrossRef]
30. Trinh, Q.N.; Lee, H.H. A new Z-source inverter topology with high voltage boost ability. *J. Electr. Eng. Technol.* **2012**, *7*, 714–723. [CrossRef]
31. Ellabban, O.; Van Mierlo, J.; Lataire, P. Control of a bidirectional Z-source inverter for electric vehicle applications in different operation. *J. Power Electron.* **2011**, *11*, 120–131. [CrossRef]